Arab J Sci Eng (2016) 41:3369–3379
DOI 10.1007/s13369-015-1904-6

RESEARCH ARTICLE - ELECTRICAL ENGINEERING

Artificial Neural Network Approach for Predicting the Water Turbidity Level Using Optical Tomography

Mohd Taufiq Mohd Khairi[1] · Sallehuddin Ibrahim[1] · Mohd Amri Md Yunus[1] · Mahdi Faramarzi[1] · Zakariah Yusuf[1]

Received: 21 April 2015 / Accepted: 6 October 2015 / Published online: 26 October 2015

Abstract Water pollution can occur with a variety of reasons such as the change in water colour, the presence of harmful bacteria and toxic waste spills. This paper presents an application of an optical tomography system based on artificial neural network (ANN) to predict the turbidity level of water sample. The system made use of the independent component analysis algorithm to calculate the K value, which indicates the attenuation value of the water turbidity level. The K value then is utilized by ANN to estimate the turbidity level. The optical tomography system can be used to evaluate the water turbidity level in the pipeline without disturbing the flow process. Evaluation of the mean square error (MSE), sum square error (SSE) and regression analysis (R) also enabled us to determine the network performance which demonstrated that the neural network is effective in inspecting the water turbidity level. The best neurone structure is revealed when two hidden layers with 20 and 10 neurones in the first and the second layer, respectively, are used. The training result shows 9.7147×10^{-7} for MSE, 0.1432 for SSE and 0.99911 for regression. For the testing part, the result for the neurone structure is 8.1473×10^{-5} for MSE, 0.7509 for SSE and 0.98525 for regression. The results revealed that the performance of ANN demonstrated a good prediction capability when the turbidity level changed. Thus, an optical tomography system with ANN proved to be an efficient tool to classify the water quality level and is beneficial to the water industry.

✉ Sallehuddin Ibrahim
salleh@fke.utm.my

[1] Department of Control and Mechatronics Engineering, Faculty of Electrical Engineering, Universiti Teknologi Malaysia, 81310 Skudai, Johor, Malaysia

Keywords Artificial neural network · Turbidity · Optical tomography

1 Introduction

Water, air and noise pollution can give bad effect to the health of human, animal and plants. This is caused by a lack of awareness among people about the dangers of pollution. Rapid technological development also contributed to an increase in the pollution statistics, especially in the city. In the pursuit of the status of a developed and high-technology country, many factors contribute to pollution. Air pollution, for example, occurred when dust and smoke from factories and vehicles are released into the air. Air pollution gives very harmful effect upon the plants. Plants suffered damage in three ways, namely necrosis (loss of leaves), chlorosis (colour change) and decreasing plant's growth [1]. Barley, cotton and apples are among the plants susceptible to damage by sulphur dioxide pollutants contained in the air. In addition, vegetable products such as tomatoes, beans and potatoes also suffered damage due to air pollution. This condition causes a shortage of quality food and creates suspicions among consumers on the safety of food resources.

Water is said to be contaminated when it experienced changes in colour, nature and shape. Contaminated water is subjected to physical and chemical changes. Physically, the presence of litter and faeces in water sources contributed to water pollution. In terms of chemistry, water pollution occurred with the presence of bacteria and microorganisms which can harm consumers. For example, water pollution caused by the rat urine viruses called "Leptospirosis" is very dangerous because it spreads quickly in the river and causes death. Therefore, the responsible authorities have taken drastic actions to close the river from public use. Other than that,

the presence of liquid such as oil spills and toxic waste also led to a decrease in the quality of water. Aquatic animals such as fishes are adversely affected since oil prevented water from absorbing oxygen. As a result, the income of fishermen is affected, and the government needs to spend a lot of money for cleaning up the oil spills.

There are many tools and techniques that can be used to measure the water turbidity level. Many types of sensor are specifically designed to identify and measure the level of turbidity level based on the physical and chemical characteristics in water. Electronic tongue has got much research attention in the last decade as a tool to monitor and analyse the quality of water which is based on the tasting sense. Two types of electronic tongues that are popularly used are potentiometric sensor and voltammetric sensor. For the potentiometric sensor, the measurement has to be made between electrodes under the conditions of no current flow. The potential energy is generated when the process for getting the equilibrium condition is conducted and redox reactions are not involved in this kind of measurement [2]. The second type of electronic tongue is the voltammetric sensor. The electrode for this sensor involved the redox reaction which is generated between two different types of electrodes. This reaction led to an increase in the current value, and this parameter is used for further analysis [2]. The determination of the water quality level can be based on the observation of the aquatic animal's behaviour such as fish since it is very sensitive to the surrounding abnormal environment. The research regarding live fish behaviour for water environmental monitoring has attracted the interest from the researchers in marine and water quality field [3–5]. Ma et al. [6] investigated the different fish trajectories in natural water and contaminated water using a charge-coupled device (CCD) camera. The experiment is conducted using several water samples from pH 5 to 9, and the abnormal rate per cycle time is obtained using artificial neural network (ANN). The result indicates that the abnormal rate per cycle time increased from the threshold rate when the fish was tested in alkaline and acidic water. Other than using live fish, many researches have successfully developed the robotic fish for water quality assessment. The main advantage is that the assessment and measurement process can be directly performed in the test field location [7]. However, the use of fish robots significantly limited the range of application. It is sufficient for deep and large reservoirs, but in shallow reservoirs, there would be problems when applying the fish robots. The problem occurred in terms of the robot's movement and swing where it would damage the propulsive stability and affect the operating reliability of sensor-based system [8].

Optical sensors are popularly used since the concept is easy and low cost. A turbidimeter investigates the optical characteristic of the light to be scattered and absorbed rather than transmitted in the straight line [9]. Several investigations have been carried out by researchers around the world for improving the current turbidimeter. Garcia et al. [10], Bilro et al. [11] and Prerana et al. [12] proposed the design of turbidimeters using optical fibres. The use of optical fibre is expanded by Aisteran et al. [13] where they applied the fibre to measure the volume and turbidity of low-viscosity fluid. Niskanen et al. [14] have successfully designed a multifunction spectrophotometer for the determination of optical properties, which enables them to control the observation of transmission, reflection and light scattering from a liquid sample. Research conducted by Lambrou et al. [15], Tai et al. [16], Ranasinghe and Ariyaratne [17], Orwin and Smart [18] and Chang et al. [19] also used optical sensors for evaluating the water turbidity level. However, the sensors have to be touched or have to be taken out from the water sample in order to measure the turbidity level. This technique is not suitable for accessing the turbidity level in the pipelines.

Tomography is known as a technique that can identify the internal characteristic of pipelines using non-destructive method. The technique is widely used in flow measurement, nuclear and chemical engineering field. In the process industries, the parameters that have investigated are concentration profiles of multi-phase flow [20], bubble flow [21], mass flow rate [22] and velocity measurement [23]. Like turbidimeter, tomography also has several sensors that can be used such as ultrasound, electronic capacitance, magnetic inductance and optical. The optical tomography system enabled us to evaluate the water turbidity level at any point in the water conveyor without disturbing the flow process. The turbidity sensor is usually marketed as a point sensor mode, which means the sensor has to collect or be placed in a water sample in order to measure the turbidity level. However, this sensor is not appropriate in flow industrial process since it cannot measure directly from the pipe and it disturbed the flow process [24]. Hence, a new design for predicting the turbidity water level is proposed using a non-invasive technique based on the use of an optical tomography system combined with an ANN approach.

2 Mathematical Modelling

This section elaborates the Beer–Lambert law for investigating the attenuation of light when the light passes through pure water and contaminated water. The algorithms applied to this experiment which consists of the independent component analysis (ICA) and ANN are also discussed.

2.1 Beer–Lambert Law

This subsection explained the modelling for predicting the turbidity level of water. Three conditions of water have been selected, which are pure water, slightly contaminated water and heavily contaminated water. Based on the Beer–Lambert

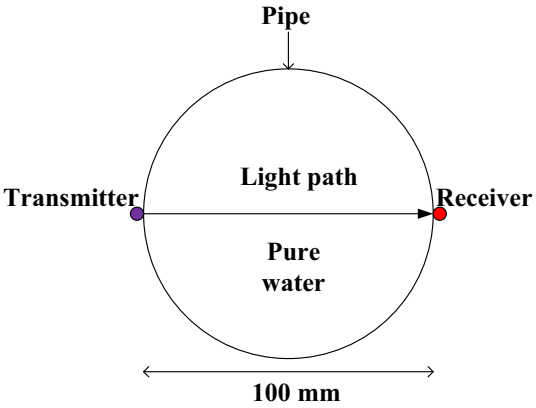

Fig. 1 Modelling of light in pure water

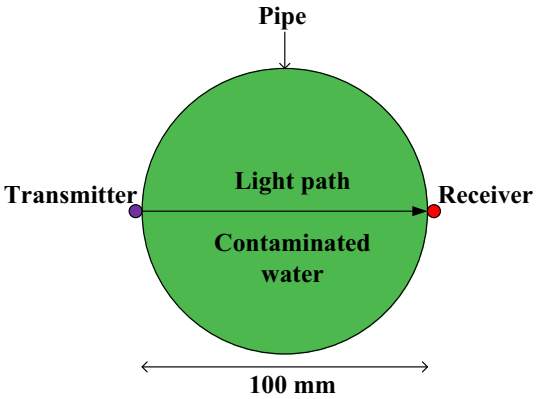

Fig. 2 The model of contaminated water

Law, the energy of light will be attenuated when it travels in different medium and distance. The Beer–Lambert law can be expressed by the following equation:

$$V_R = V_T \exp[-(\alpha l)] \tag{1}$$

where V_R, the receiving sensor voltage; V_T, the initial transmitted voltage; l is the path length of liquid medium (mm); α, attenuation coefficient for material (mm^{-1}).

The model for light path in pure water is shown in Fig. 1. The attenuation coefficient for water is $\alpha = 0.0287\,mm^{-1}$ [25]. Light will be transmitted through water contained in a pipe having a diameter of 100 mm, and the length of path light is considered equal to the diameter of the pipe. In this experiment, the medium in the pipe is water. Supposed the value of the transmitting voltage, V_T, is 5 V. Hence, the equation for the receiver voltage, V_R, can be written as:

$$V_R = 5\exp[-(0.0287)(100)] \tag{2}$$
$$V_R = 5[0.0567] \tag{3}$$
$$V_R = 0.2835\,V \tag{4}$$

The energy of light is attenuated when it passes through water. The estimation of water quality level is based on the value of the receiver voltage, V_R, and it is a function of the exponential value. For contaminated water, the pure water is polluted by adding the green colour of food ingredients which resembles the contaminants. This modelling will emphasize on the effect of the attenuation coefficient value when optical light passed through the contaminated water. The attenuation coefficient for the water medium is expected to decrease when the water is contaminated. It is because the light energy has been absorbed by water and hence affects the attenuation coefficient value. The model for contaminated water is shown in Fig. 2. Let the new coefficient for the slightly contaminated water be $0.0263\,mm^{-1}$. The Beer–Lambert's law equation can be expressed as:

$$V_R = 5\exp[-(0.0263)(100)] \tag{5}$$
$$V_R = 5[0.0721] \tag{6}$$
$$V_R = 0.3603\,V \tag{7}$$

Let the new coefficient for the heavily contaminated water be $0.0250\,mm^{-1}$. The Beer–Lambert's law equation can be expressed as:

$$V_R = 5\exp[-(0.0250)(100)] \tag{8}$$
$$V_R = 5[0.0821] \tag{9}$$
$$V_R = 0.4105\,V \tag{10}$$

By comparing all cases, it can be observed that the exponential value for the contaminated water model is higher than the pure water model, and the value of receiver voltage, V_R, is a function of the exponential value.

2.2 Algorithm Method

In this section, the concept and implementation of ICA and ANN algorithms are elaborated briefly. The previous studies regarding both algorithms are also discussed.

2.2.1 Independent Component Analysis

Independent component analysis was introduced in 1990 as a method that can separate an independent source from a linear mixture and solve the mixed signal problem [26]. It is widely used in many fields such as biomedical [27], signal processing [28] and water quality estimation [29]. ICA can be expressed as:

$$X = AS \tag{11}$$

where X is the matrix of source signals mixture, A is the mixing matrix, and S is the matrix denoting a source signal. The aim is to recover S and the process started by obtaining

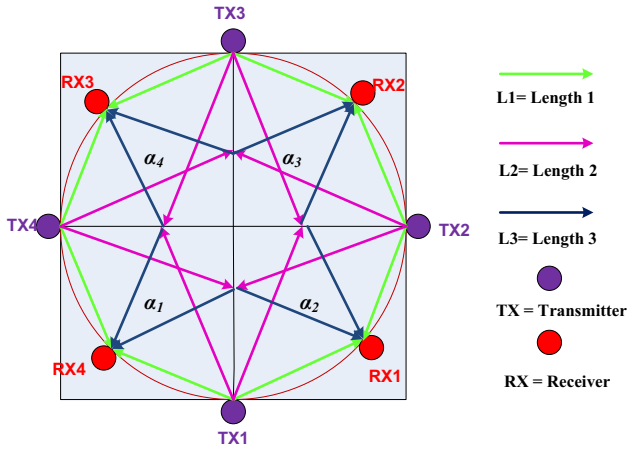

Fig. 3 Model of four sensor's pair with four pixels

the separating matrix, W where $W = A^{-1}$. Hence, the independent source, $\hat{S}$, can be obtained by:

$$\hat{S} = WX \tag{12}$$

The parameter of interest is W since it contained the attenuation coefficient (α) and it is related to the turbidity factor (M). ICA is implemented in this research in order to extract the transmitters' signal which is detected by the receiver. Eighteen transmitters and eighteen receivers are used where the sensors are mounted surrounding the pipelines. Therefore, a total of 324 pixels (18 × 18 pixels) are formed using ICA. But, the measurement of K value is considered for the pixels which are in the pipe cross section only. Hence, only 280 pixels are taken for measurement consideration since the rest of the pixels are outside the pipe. The calculation procedure for getting the K value which indicated the attenuation value is elaborated in [30].

For simplicity, the modelling for the algorithm is described using four transmitters and four receivers, while the actual system consists of eighteen transmitters and eighteen receivers as shown in Fig. 3. It is because, the explanation of the ICA concept using eighteen pairs of sensors is complex to explain since the matrix equation is too long. Hence, four pairs of sensors and four absorptions coefficients are chosen. Transmitters 1, 2, 3 and 4 are represented as TX1, TX2, TX3 and TX4, while receivers 1, 2, 3 and 4 are represented as RX1, RX2, RX3 and RX4. The attenuation coefficients are represented as α_1, α_2, α_3 and α_4.

In this model, each receiver is supposed to detect light from all transmitters. Take for example receiver RX1. The four signals received at RX1 have been mixed where each light has its own characteristics such as the light length and the absorption coefficient. The equation of receiver RX1 voltage, V_{R1}, can be written as:

$$\begin{aligned} V_{R1} = {} & V_{T1}\exp(-\propto_2 l_1) + V_{T2}\exp(-\propto_2 l_1) \\ & + V_{T3}\exp(-\propto_3 l_2) + V_{T3}\exp(-\propto_2 l_3) \\ & + V_{T4}\exp(-\propto_1 l_2) + V_{T4}\exp(-\propto_2 l_3) \end{aligned} \tag{13}$$

where V_{T1} is transmitter TX1 voltage, V_{T2} is transmitter TX2 voltage, V_{T3} is transmitter TX3 voltage, V_{T4} is transmitter TX4 voltage, α_1 is the attenuation coefficient for material 1, α_2 is the attenuation coefficient for material 2, α_3 is the attenuation coefficient for material 3, and α_4 is the attenuation coefficient for material 4, l_1 is length 1, l_2 is length 2, and l_3 is length 3. Equation (13) can be arranged as:

$$\begin{aligned} V_{R1} = {} & V_{T1}\exp(-\propto_2 l_1) + V_{T2}\exp(-\propto_2 l_1) \\ & + V_{T3}\exp(-\propto_3 l_2 - \propto_2 l_3) \\ & + V_{T4}\exp(-\propto_1 l_2 - \propto_2 l_3) \end{aligned} \tag{14}$$

The equations for receiver RX2 voltage, receiver RX3 voltage and receiver RX4 voltage are simplified as:

$$\begin{aligned} V_{R2} = {} & V_{T1}\exp(-\propto_2 l_2 - \propto_3 l_3) + V_{T2}\exp(-\propto_3 l_1) \\ & + V_{T3}\exp(-\propto_3 l_1) \\ & + V_{T4}\exp(-\propto_4 l_2 - \propto_3 l_3) \end{aligned} \tag{15}$$

$$\begin{aligned} V_{R3} = {} & V_{T1}\exp(-\propto_1 l_2 - \propto_4 l_3) \\ & + V_{T2}\exp(-\propto_3 l_2 - \propto_4 l_3) + V_{T3}\exp(-\propto_4 l_1) \\ & + V_{T4}\exp(-\propto_4 l_1) \end{aligned} \tag{16}$$

$$\begin{aligned} V_{R4} = {} & V_{T1}\exp(-\propto_1 l_1) + V_{T2}\exp(-\propto_2 l_2 - \propto_1 l_3) \\ & + V_{T3}\exp(-\propto_4 l_2 - \propto_1 l_3) \\ & + V_{T4}\exp(-\propto_1 l_1) \end{aligned} \tag{17}$$

Equations (14) until (17) can be transformed into matrix as shown in Eq. (18), where X is a matrix of mixture of source signals, represented by the voltage receiver (V_R). The $\exp(-\alpha l)$ is symbolized as a mixing matrix (A), and voltage transmitter (V_T) is signified as a source signal (S).

$$\begin{matrix} X & = & & A & & & S \end{matrix}$$
$$\begin{bmatrix} V_{R1} \\ V_{R2} \\ V_{R3} \\ V_{R4} \end{bmatrix} = \begin{bmatrix} e^{-\propto_2 l_1} & e^{-\propto_2 l_1} & e^{-\propto_3 l_2 - \propto_2 l_3} & e^{-\propto_1 l_2 - \propto_2 l_3} \\ e^{-\propto_2 l_2 - \propto_3 l_3} & e^{-\propto_3 l_1} & e^{-\propto_3 l_1} & e^{-\propto_4 l_2 - \propto_3 l_3} \\ e^{-\propto_1 l_2 - \propto_4 l_3} & e^{-\propto_3 l_2 - \propto_4 l_3} & e^{-\propto_4 l_1} & e^{-\propto_4 l_1} \\ e^{-\propto_1 l_1} & e^{-\propto_2 l_2 - \propto_1 l_3} & e^{-\propto_4 l_2 - \propto_1 l_3} & e^{-\propto_1 l_1} \end{bmatrix} \begin{bmatrix} V_{T1} \\ V_{T2} \\ V_{T3} \\ V_{T4} \end{bmatrix} \tag{18}$$

ICA is utilized to separate the mixture of source signals where in Eq. (19), the matrix position of source signals (S), represented as V_T, is interchanged with V_R denoted by matrix of mixture of source signals (X). The separating matrix (W) is formed to replace the mixing matrix (A) where theoretically, W is obtained by the inversing process of A.

$$\begin{matrix} \hat{S} & = & W & & X \end{matrix}$$
$$\begin{bmatrix} V_{T1} \\ V_{T2} \\ V_{T3} \\ V_{T4} \end{bmatrix} = \begin{bmatrix} W_{1,1} & W_{1,2} & W_{1,3} & W_{1,4} \\ W_{2,1} & W_{2,2} & W_{2,3} & W_{2,4} \\ W_{3,1} & W_{3,2} & W_{3,3} & W_{3,4} \\ W_{4,1} & W_{4,2} & W_{4,3} & W_{4,4} \end{bmatrix} \begin{bmatrix} V_{R1} \\ V_{R2} \\ V_{R3} \\ V_{R4} \end{bmatrix} \quad (19)$$

In this case, the parameter considered for computing the water turbidity level is the matrix A. However, the matrix cannot be acquired directly from the ICA method. Hence, the related parameter regarding $A$is supported where matrix W is obtained as an inverse process in order to find the matrix A. Matrix W is inversed first before calculating the value of K. S is a source signal which it obtained before ICA is applied to the system. $\hat{S}$ is an estimation of the source signal which is obtained after ICA is utilized. The matrix shown in Eq. (18) is formed in an arbitrary row after utilizing the ICA and the $\hat{S}$ value represented as V_T can assist in rearranging the matrix row. V_T is set by a peripheral interface controller (PIC) microcontroller to have different pulse duration values. Hence, the rearrangement of the matrix's row is according to the order of V_T from 1 ms until 18 ms. The error in the estimating process using ICA sometimes occurred when the 18 transmitter's signal is not separated properly [31]. From 18 transmitters' signals, the ICA algorithm sometimes separated 17 or 16 signals only. This problem can be solved by rearranging manually the row of matrix W for the missing signals. Among the most widely used ICA algorithms are FastICA and Infomax. This research implemented the FastICA algorithm which provides recovery of independent sources by employing the higher-order statistics, and the estimation process is done one by one [31]. The algorithm separates the source signals based on their non-Gaussianity, and it finds one independent component at a time instead of solving the mixing matrix [28]. The advantages of FastICA are it is parallel, simple for computation process and requires small memory size [32].

2.2.2 *Artificial Neural Network*

Artificial neural network (ANN) is a tool that can deal with uncertainty and complexity of the system. The tool is very suitable and appropriate to use for nonlinear function prediction and can produce the good estimation process even if the data are complex [33]. The artificial neurones are the computing elements of neural networks and cooperate to perform the desired task. The neurone is expressed in terms of the McCulloch Pitt's model:

$$\gamma = \sum_{i=1}^{k} w_i x_i + \beta \quad (20)$$

where k is the number of inputs, w is the weight associated with the ith input x_i, and β is the bias. The output y is given by:

$$y = g(\gamma) \quad (21)$$

The ANN approach has been introduced recently in the water monitoring field. ANN provides an alternative way to overcome high cost and time consumption for predicting the water quality [34]. Iglesias et al. [34] accessed the water turbidity level in the Nalón River basin (Northern Spain) by using ANN. The turbidity level is predicted from ammonium, conductivity, dissolved oxygen and pH. These parameters were tested with two types of condition: with temperature consideration and no temperature consideration. The results showed that the different temperature levels affected the process of turbidity estimation. The results also indicated that the turbidity estimation process performs better when the temperature is considered. Khalil et al. [35] investigated the application of neural network for estimating the water quality in Nile Delta, Egypt. The structures of ANN model such as inputs, hidden layer and nodes of hidden layer were varied in order to get the best output result. The result of the ANN model is compared with the linear regression model which showed that the ANN model performed better in terms of accuracy.

Bayram et al. [36] used feed-forward ANN for predicting the suspended sediment concentration (SSC) from six sampling stations in the Eastern Black Sea Basin, Turkey. The output result is compared between ANN and the regression analysis (RA). The total data used for the ANN modelling were 144 data. Out of this number, 108 data were used for training, 24 for testing and 12 for validation. ANN indicated a better result by showing smaller root mean square (RMSE) and mean absolute error (MAE) of 11.40 and 17.87, respectively. Meanwhile, the RA method showed 19.12 for RMSE and 25.09 for MAE. Gazzaz et al. [37] predicted the water quality index (WQI) using ANN in eight measurement station in Kinta River, Malaysia. Twenty-three water quality parameters such as water colour, pH, salinity, dissolve oxygen were taken for sampling. A three-layer perceptron network is used for this study which comprised one input layer, one hidden layer and the output layer. This study also employed a parallel, fully connected and feed-forward network to obtain a nonlinear regression model for estimating the WQI. The result showed that the optimal network for the ANN model is 23-34-1 which means 23 inputs, 34 neurones of hidden layer and a single output. The combination of

Table 1 Neural network performance from previous study

Network structure	Parameters	Performance	Reference
Feed-forward 6-70-1	Ammonium, conductivity dissolve oxygen (DO), pH and temperature values	$R^2 = 0.7$ $R^2 = 0.8$	Iglesias et al. [34]
Feed-forward 2-3-1	Dissolved oxygen (DO), biological oxygen demand (BOD), chemical oxygen demand (COD)	RMSE = 68.2	Khalil et al. [35]
Feed-forward 3-3-2	Suspended sediment concentration (SSC)	MAE = 11.40 RSME = 17.87	Bayram et al. [36]
Feed-forward 23-34-1	Water colour, pH, salinity, dissolve oxygen (DO), chemical oxygen demand (COD), total solids (TS)	$r = 0.977$ $R^2 = 0.95$	Gazzaz et al. [37]
Hopfield structure	Biological oxygen demand (BOD), permanganate index, ammonia nitrogen, copper (Cu), zinc (Zn)	MSE = 9.8463×10^{-7}	Chu et al. [38]
Feed-forward 5-100-20	Dissolved oxygen (DO), turbidity Water colour, pH, oxidability, ammonia nitrogen, conductivity	RSME = 0.49 $r = 0.84$	Rak [39]
Feed-forward 6-12-1	Turbidity, pH, temperature values transmembrane pressure	MSE = 2.16×10^{-4} RMSE = 2.16×10^{-2} $r = 0.8295$	Kabsch-Korbutowicz and Kutylowska [40]

this network with the quick propagation training algorithm provided a high correlation, $r = 0.977$, and coefficient of determination, $R^2 = 95.4\,\%$.

Chu et al. [38] developed the factor analysis and Hopfield neural network method to access the water quality in Liao River, China. The work involved analysing the samples for total nitrogen (TN), total phosphorus (TP), dissolved oxygen (DO), biochemical oxygen demand (BOD_5), etc. The result indicated that the combination of factor analysis and Hopfield neural network method is much better than the Hopfield neural network alone in effectively reducing the degree of Hopfield neural network over-fitting. Rak [39] proposed a Bayesian model of neural networks and Gaussian processes to estimate the water treatment turbidity in a newly operating water treatment system at the Sosnówka reservoir, Poland. Kabsch-Korbutowicz and Kutylowska [40] implemented ANN for predicting water quality after implementing the coagulation/ultrafiltration processes in an immersed membrane. The performances of the various neural network models are summarized in Table 1.

The network structure and network specification are two major steps for designing the ANN. The network structure determines the numbers for layer and neurones for input, hidden and output phase. The network specification covers the classification of the training algorithm, value of learning rate, value of momentum rate, number of iterations and training stop criteria [37]. Although there are many different factors that may affect the ANN modelling, only two factors were studied in this experiment which are the number of hidden layers and the number of neurones in the hidden layer. The back-propagation (BP) algorithm and Hopfield neural networks (HNN) are commonly used to assess water quality. The structure of neural network can be classified to feed-forward and recurrent neural network. Feed-forward neural network structure has unidirectional flow of information as illustrated in Fig. 4. The recurrent neural network is any network whose neurones send feedback signals to each other. BP is made up of a large number of interconnected neurones which contain three types of layers: input, hidden and output layer. Each neurone in the input layer is connected to all neurones in the hidden layer. Besides, all the neurones in the hidden layer are connected to the output neurones. This network structure is named as multi-layer perceptron (MLP) since there is no connection between the neurones in the same layer. The input signal is sent forward to the neurones in the hidden layer. The network will send back the signal if any errors existed, whereas at the same time, the optimization of the weight is performed in order to get the best output [41].

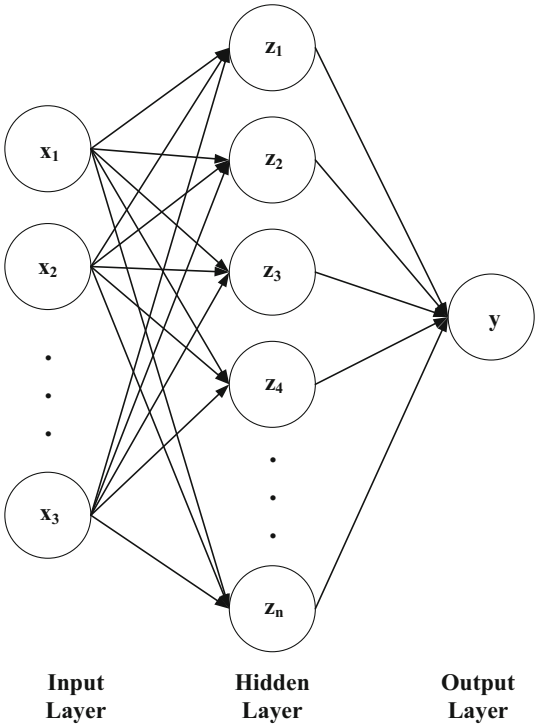

Fig. 4 Feed-forward neural network structure

3 Experimental Set-up

The experiment used a vertical transparent acrylic pipe with a diameter of 100 mm and a height of 680 mm. Eighteen light-emitting diodes (LED) acting as transmitters and eighteen photodiodes acting as receivers are mounted around the pipe using a sensor jig. An infrared light with a wavelength of 940 nanometer (nm) is chosen to increase the accuracy of measurement in order to minimize the disturbance from the laboratory lamp. When light is transmitted through the pipe, it will be sensed by the receiver but the voltage amplitude sensed by the receiver is too low to be analysed. Hence, a signal conditioning circuit which contained an operational amplifier is added to amplify the voltage amplitude. The Agilent U2331A data acquisition system was used to capture the data and transfer it into the computer. The DAS has 64 single-ended/32 digital input multiplex analogue input channels, 3 MSa/s sampling rate for 1 channel and up to 1 MSa/s sampling rate for multiple channels. The ICA and ANN algorithms were programmed using the LabVIEW and MATLAB software, and the output data are acquired and analysed. The set-up for the measurement system is shown in Fig. 5. The transmitters (TX) and receivers (RX) are illustrated in purple and red colour, respectively. The experiment for estimating the water turbidity level is done by polluting 3 litres (l) of pure water with several volumes of green food colouring; 0 ml means the water sample is clean water. The samples of contaminated water were prepared by adding several volumes of food colouring starting from 2 ml, followed by 5, 7, 11, 15, 21, 25, 30, 35, 37 and 42 ml. As such 12 different volumes of food colouring were tested. Figure 6 shows the water sample which was contaminated by 35 ml of food colouring. Each volume was measured 40 times in order to obtain as much data as possible for neural network process. Hence, we have 480 measurement data. 10 pixels are picked

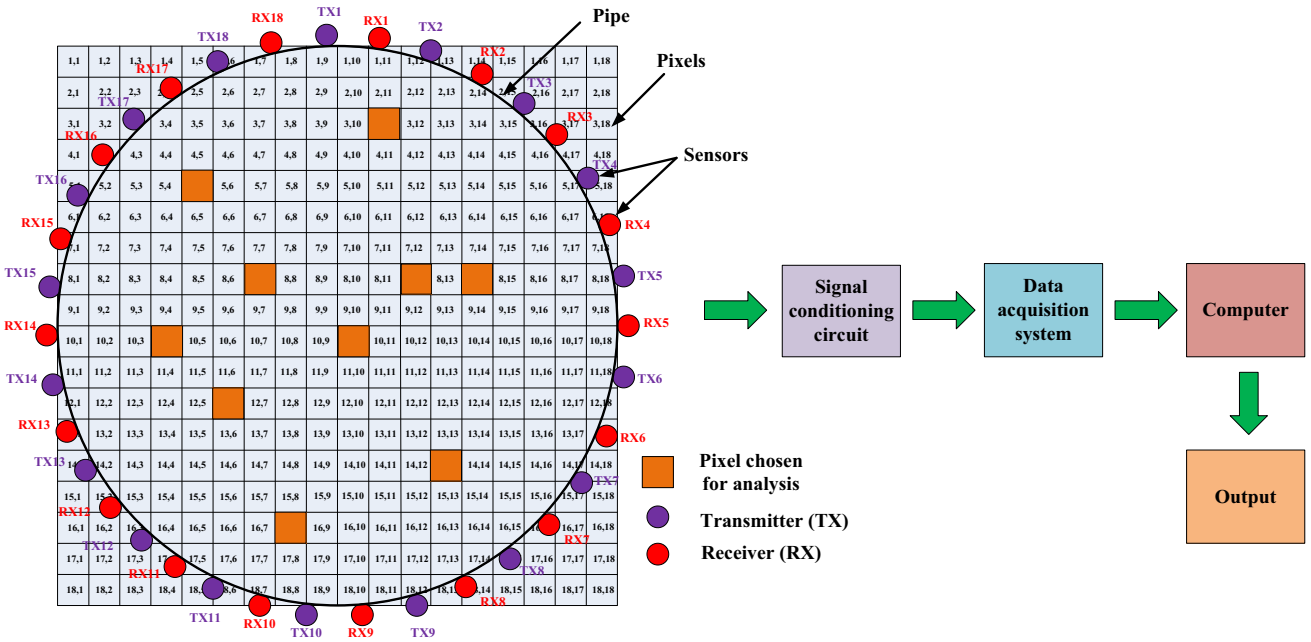

Fig. 5 The experimental set-up

Fig. 6 The sample of water contaminated by 35 ml of food colouring

randomly in order to analyse the K value as shown by the orange squares in Fig. 5. Out of 480 measurements data, 70 % are selected for training (336 data). Meanwhile, 20 % are for testing (96 data) and 10 % are for validation (48 data). The data were normalized between 0 and 1 to improve the performance of the network.

4 Result and Discussion

The number of layers and neurones for the hidden layers was varied in order to find the best network performance. The network performance of ANN model is assessed by observing the mean square error (MSE), sum square error (SSE) and regression (R) for different settings of hidden layer. The parameters are calculated as follows:

$$\mathrm{MSE} = \frac{1}{N}\sum_{i=1}^{N}(x_i - y_i)^2 \tag{22}$$

$$\mathrm{SSE} = \sum_{i=1}^{N}(x_i - y_i)^2 \tag{23}$$

$$R = \frac{\sum_{i=1}^{N}(x_i - \bar{x}_i)(y_i - \bar{y}_i)}{\sqrt{\left(\sum_{i=1}^{N}(x_i - \bar{x}_i)^2\right)\left(\sum_{i=1}^{N}(y_i - \bar{y}_i)^2\right)}} \tag{24}$$

Table 2 Performance of network structure

Hidden		Mean square error (MSE)		Sum square error (SSE)		Regression (R)	
Layer	Neurones	Training	Testing	Training	Testing	Training	Testing
1	10	7.0501×10^{-6}	2.4045×10^{-4}	1.0396	2.2160	0.99571	0.98805
	15	4.3738×10^{-7}	1.0291×10^{-4}	0.0645	0.9484	0.99719	0.98863
	20	3.7095×10^{-7}	1.1789×10^{-7}	0.0547	1.0864	0.99743	0.98715
2	[10,10]	1.1144×10^{-7}	5.4632×10^{-4}	0.0164	5.0349	0.99672	0.98094
	[15,10]	3.5213×10^{-6}	3.3682×10^{-4}	0.5192	3.1041	0.99747	0.98674
	[20,10]	$\mathbf{9.7147 \times 10^{-7}}$	$\mathbf{8.1473 \times 10^{-5}}$	**0.1432**	**0.7509**	**0.99911**	**0.98525**

Bold values indicate the best performance of neural network structure

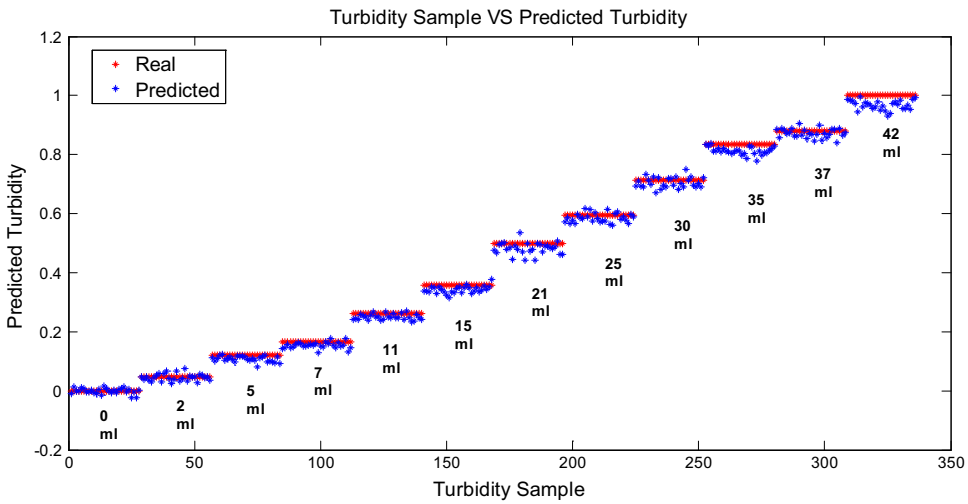

Fig. 7 Training phase performance of the turbidity measurement

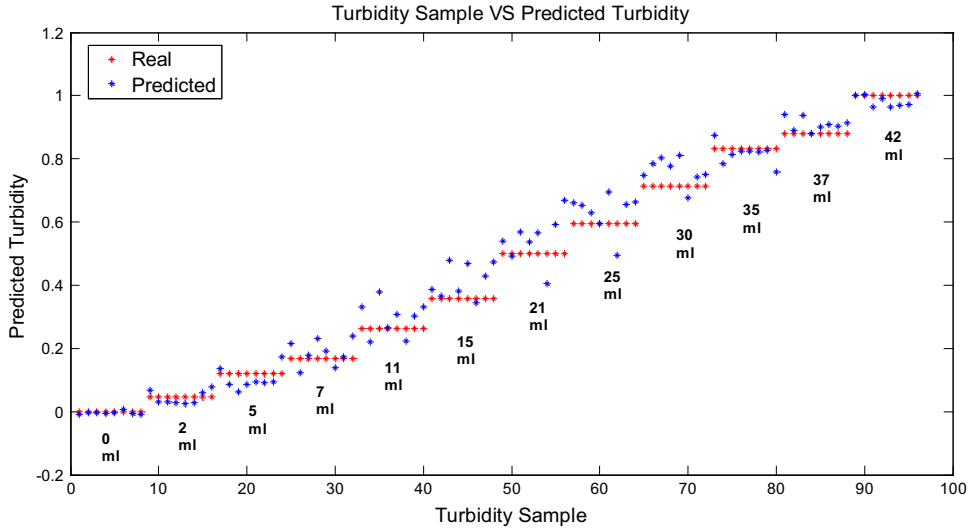

Fig. 8 Testing phase performance of the turbidity measurement

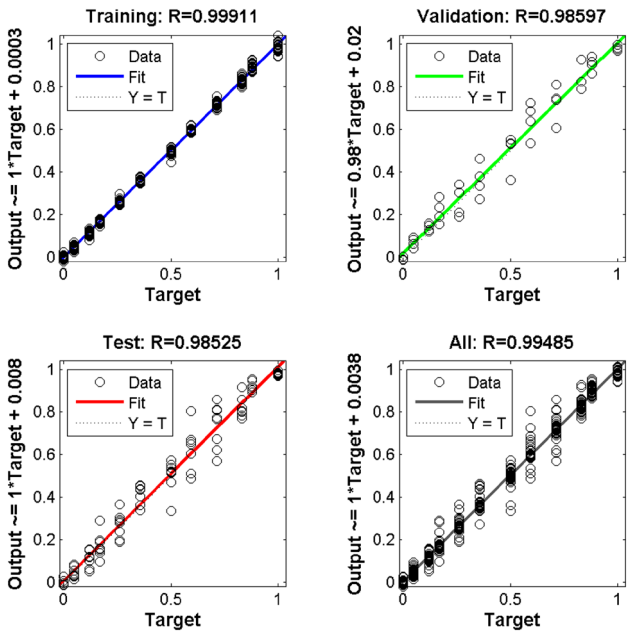

Fig. 9 Regression plot for network structure 10-[20,10]-1

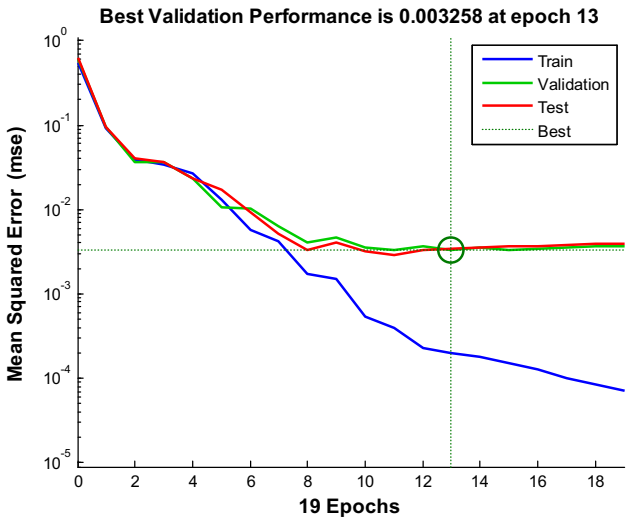

Fig. 10 Performance plot for training, validation and testing phase

where x_i is the i^{th} measured value, y_i is the predicted value, $\bar{x}_i$ is the mean of the measured values, $\bar{y}_i$ is the mean of the predicted value, and N is the number of samples. The results of the network performance are presented in Table 2. After repeated tests, the two hidden layers with 20 neurones in the first layer and 10 neurones in the second layer provided the best performance. It can be noted from Table 2 that the MSE value for the network structure of 10-[20,10]-1 is 9.7147×10^{-7} for training and 8.1473×10^{-5} for testing. However, the SSE performance for this structure does not give a good result with 0.1432 and 0.7509 for training and testing, respectively. Figures 7 and 8 show the prediction performances of the turbidity measurement for the network structure of 10-[20,10]-1 during training and testing, respectively. The turbidity level of water being investigated was from 0 ml until 42 ml.

The predicted turbidity values of ANN model are in good agreement with the real value, thus demonstrating its effectiveness in predicting the turbidity level during training and testing. The regression analysis is performed to find the correlation between the network output and the corresponding target. The best regression value is pointed out by network structure of 10-[20,10]-1 with 0.99485 for total response as shown in Fig. 9 indicating a very strong correlation. During the training, R is 0.99911 which is higher compared with the other structure and R is 0.98525 for testing. This result shows the correlation is quite strong which shows that a reliable prediction could be achieved. Figure 10 shows the performance plot which contained the training plot, the vali-

dation plot and the test plot. The best validation performance occurred at epoch 13 in which the MSE for validation is 0.003258.

5 Conclusion

The paper presented an estimation process of the water turbidity level using an optical tomography measurement system based on a feed-forward neural network. The K value obtained by the ICA algorithm has been predicted and analysed by the neural network approach. The results demonstrated that the neural network is effective in inspecting the water turbidity level. The various numbers of hidden layers and neurones are evaluated in order to find the best network performance. The network structure containing two hidden layers with 20 and 10 neurones in the first and the second layer, respectively, has shown the best network structure by providing the training result of 9.7147×10^{-7} for mean square error, 0.1432 for sum square error and 0.99911 for regression. The testing result also gives a promising outcome with 8.1473×10^{-5} for MSE, 0.7509 for SSE and 0.98525 for regression. Hence, the neural network model based on the optical tomography system may function as a valuable predicting tool for the water quality measurement.

Acknowledgments The authors would like to acknowledge the assistance of the Higher Education Ministry and Universiti Teknologi Malaysia for providing the research Grant 05H67 which enabled this research to be carried out.

References

1. Darral, N.M.: The effect of air pollutants on physiological processes in plants. Plant Cell Environ. **12**, 1–30 (1989)
2. Krantz-Rülcker, C.; Stenberg, M.; Winquist, F.; Lundström, I.: Electronic tongues for environmental monitoring based on sensor arrays and pattern recognition: a review. Anal. Chim. Acta. **426**, 217–226 (2001)
3. Kuklina, I.; Kouba, A.; Kozák, P.: Real-time monitoring of water quality using fish and crayfish as bio-indicators: a review. Environ. Monit. Assess. **185**(6), 5043–5053 (2013)
4. Steig, T.W.; Johnston, S.V.: Monitoring fish movement patterns in a reservoir using horizontally scanning split-beam techniques. ICES J. Mar. Sci. **53**, 435–441 (1996)
5. Serra-Toro, C.; Montoliu, R.; Traver, V. J.; Hurtado-Melgar, I. M.; Nunez-Redo, M.; Cascales, P.: Assessing water quality by video monitoring fish swimming behavior. In: 2010 20th International Conference on Pattern Recognition. Istanbul, Turkey, pp. 428–431 (2010)
6. Ma, H.; Tsai, T.-F.; Liu, C.-C.: Real-time monitoring of water quality using temporal trajectory of live fish. Expert Syst. Appl. **37**(7), 5158–5171 (2010)
7. Yang, G.-H.; Ryuh, Y.: Design of high speed fish-like robot "Ichthus V5.7." In: 2013 10th International Conference on Ubiquitous Robots and Ambient Intelligence (URAI). Jeju, South Korea, pp. 451–453 (2013)
8. Liu, Y.; Chen, W.; Liu, J.: Research on the swing of the body of two-joint robot fish. J. Bionic Eng. **5**, 159–165 (2008)
9. Omar, A.F.B.; Matjafri, M.Z.B.: Turbidimeter design and analysis: a review on optical fiber sensors for the measurement of water turbidity. Sensors **9**(10), 8311–8335 (2009)
10. Garcia, A.; Perez, M.A.; Ortega, G.J.G.O.; Dizy, J.T.: A new design of low-cost four-beam turbidimeter by using optical fibers. IEEE Trans. Instrum. Meas. **56**(3), 907–912 (2007)
11. Bilro, L.; Prats, S.A.; Pinto, J.L.; Keizer, J.J.; Nogueira, R.N.: Design and performance assessment of a plastic optical fibre-based sensor for measuring water turbidity. Meas. Sci. Technol. **21**(10), 1–4 (2010)
12. PreranaShenoy, M.R.; Pal, B.P.; Gupta, B.D.: Design, analysis, and realization of a turbidity sensor based on collection of scattered light by a fiber-optic probe. IEEE Sens. J. **12**(1), 44–50 (2012)
13. Aiestaran, P.; Arrue, J.; Zubia, J.: Design of a sensor based on plastic optical fibre (POF) to measure fluid flow and turbidity. Sensors **9**, 3790–3800 (2009)
14. Niskanen, I.; Räty, J.; Peiponen, K.-E.: A multifunction spectrophotometer for measurement of optical properties of transparent and turbid liquids. Meas. Sci. Technol. **17**(12), 87–91 (2006)
15. Lambrou, T.P.; Anastasiou, C.C.; Panayiotou, C.G.: A nephelometric turbidity system for monitoring residential drinking water quality. In: Komninos, N. Sensor Applications, Experimentation, and Logistics, pp. 43–55. Springer, Heidelberg (2010)
16. Tai, H.; Li, D.; Wang, C.; Ding, Q.; Wang, C.; Liu, S.: Design and characterization of a smart turbidity transducer for distributed measurement system. Sens. Actuators A Phys. **175**, 1–8 (2012)
17. Ranasinghe, D.M.A.; Ariyaratne, T.R.: Design and construction of cost effective turbidimeter to be used in water purification plants in Sri Lanka. In: Proceedings of the Technical Sessions, Kelaniya, Sri Lanka. pp. 65–70 (2012)
18. Orwin, J.F.; Smart, C.C.: An inexpensive turbidimeter for monitoring suspended sediment. Geomorphology **68**, 3–15 (2005)
19. Chang, C.C.; Wu, C.T.; Lin, Y.B.; Gu, M.H.: Water velocimeter and turbidity-meter using visible light communication modules. In: 2013 IEEE Sensors, pp. 1–4, Baltimore, MD, USA (2013)
20. Ismail, I.; Gamio, J.C.; Bukhari, S.F.A.; Yang, W.Q.: Tomography for multi-phase flow measurement in the oil industry. Flow Meas. Instrum. **16**, 145–155 (2005)
21. Ibrahim, S.; Yunus, M.A.M.; Green, R.G.; Dutton, K.: Concentration measurements of bubbles in a water column using an optical tomography system. ISA Trans. **51**(6), 821–826 (2012)
22. Zheng, Y.; Liu, Q.: Review of techniques for the mass flow rate measurement of pneumatically conveyed solids. Measurement **44**(4), 589–604 (2011)
23. Liu, S.; Chen, Q.; Wang, H.; Jiang, F.; Ismail, I.; Yang, W.: Electrical capacitance tomography for gas–solids flow measurement for circulating fluidized beds. Flow Meas. Instrum. **16**, 135–144 (2005)
24. Khairi, M.T.M.; Ibrahim, S.; Yunus, M.A.M.; Faramarzi, M.: A review on the design and development of turbidimeter. Sens. Rev. **35**(1), 98–105 (2015)
25. Daniels, A.R.: Dual modality tomography for the monitoring of constituent volumes in multi-component flows. Ph.D. Thesis (1996)
26. Chen, J.; Wang, X.Z.: A New Approach to near-infrared spectral data analysis using independent component analysis. J. Chem. Inf. Comput. Sci. **41**, 992–1001 (2001)
27. James, C.J.; Hesse, C.W.: Independent component analysis for biomedical signals (Topical Review). Pysiol. Meas. **26**(1), R15–R39 (2005)
28. Wang, G.; Ding, Q.; Hou, Z.: Independent component analysis and its applications in signal processing for analytical chemistry. Trends Anal. Chem. **27**(4), 368–376 (2008)
29. Yunus, M.A.M.; Mukhopadhyay, S.C.; Ibrahim, S.: Planar electromagnetic sensor based estimation of nitrate contamination in

water sources using independent component analysis. IEEE Sens. J. **12**(6), 2024–2034 (2012)
30. Khairi, M.T.M.; Ibrahim, S.; Yunus, M,A,M.; Sulaiman, M.N.M.: An application of independent component analysis method for estimating the quality level of water using optical tomography. In: 2013 IEEE 4th Control and System Graduate Research Colloquium. Shah Alam, Malaysia (2013)
31. Naik, G.R.; Kumar, D.K.: An overview of independent component analysis and its applications. Informatica **35**, 63–81 (2011)
32. Hyvärinen, A.; Oja, E.: Fast and robust fixed-point algorithms for independent component analysis. IEEE Trans. Neural Networks. **10**(3), 626–634 (1999)
33. Gaya, M.S.; Abdul Wahab, N.; Sam, Y.M.; Samsudin, S.I.; Jamaludin, I.W.: Comparison of NARX neural network and classical modelling approaches. Appl. Mech. Mater. **554**, 360–365 (2014)
34. Iglesias, C.; Martínez Torres, J.; García Nieto, P.J.; Alonso Fernández, J.R.; Díaz Muñiz, C.; Piñeiro, J.I.; Taboada, J.: Turbidity prediction in a River Basin by using artificial neural networks: A case study in Northern Spain. Water Resour. Manag. **28**, 319–331 (2014)
35. Khalil, B.M.; Awadallah, A.G.; Karaman, H.; El-Sayed, A.: Application of artificial neural networks for the prediction of water quality variables in the Nile Delta. J. Water Resour. Prot. **4**, 388–394 (2012)
36. Bayram, A.; Kankal, M.; Onsoy, H.: Estimation of suspended sediment concentration from turbidity measurements using artificial neural networks. Environ. Monit. Assess. **184**, 4355–4365 (2012)
37. Gazzaz, N.M.; Yusoff, M.K.; Aris, A.Z.; Juahir, H.; Ramli, M.F.: Artificial neural network modeling of the water quality index for Kinta River (Malaysia) using water quality variables as predictors. Mar. Pollut. Bull. **64**(11), 2409–2420 (2012)
38. Chu, H.B.; Lu, W.X.; Zhang, L.: Application of artificial neural network in environmental water quality assessment. J. Agric. Sci. Tech. **15**, 343–356 (2013)
39. Rak, A.: Water turbidity modelling during water treatment processes using artificial neural networks. Int. J. Water Sci. **2**(3), 1–10 (2013)
40. Kabsch-Korbutowicz, M.; Kutylowska, M.: Use of artificial intelligence in predicting the turbidity retention coefficient during ultrafiltration of water. Environ. Prot. Eng. **37**(2), 75–84 (2011)
41. Gaya, M.S.; Abdul Wahab, N.; Samsudin, S.I.: ANFIS modelling of carbon and nitrogen removal in domestic wastewater treatment plant. J. Teknol. **67**(5), 29–34 (2014)